Particle Simulation of Plasma Energy Deposition on Hollow Cathode Insert

IEPC-2017-343

Presented at the 35th International Electric Propulsion Conference
Georgia Institute of Technology • Atlanta, Georgia • USA
October 8 – 12, 2017

Shuai Cao[1], Junxue Ren[2] and Haibin Tang[3]
Beihang University, Beijing, 100083, China

Abstract: A two-dimensional axisymmetric plasma simulation model has been employed to investigate the discharge parameters and plasma energy transfer in the hollow cathode (HC) insert region. These issues involved in the physical process of hollow cathode discharge were studied by adopting the Particle-in-cell (PIC) numerical method combined with Monte-Carlo collisions. This approach established a particle motion and energy exchange model to record the microscopic characteristics of particles. The distributions of plasma potential, density and energy flux deposition of particles hitting the emitter surface are presented in this paper when cathode operated at a discharge current of 13.0A, and mass flow rate of 3.7sccm. The simulation results predict a non-Maxwellian electron energy distribution in the insert region. As the orifice size increases, the plasma potential of ionization region, sheath potential, and ion heating flux increase markedly while plasma density, electron heating flux, and emitter temperature have the opposite trends. It indicates that the particle behaviors connected with the increased orifice size could result in the reduced dissipation rate and the enhanced sputtering erosion of the emitter materials.

Nomenclature

A	=	emitter surface area
d_0	=	orifice diameter
D	=	constant
e	=	elementary charge
$E_{e,kinetic}$	=	electron kinetic energy
$E_{i,kinetic}$	=	ion kinetic energy
$E_{e,sheath}$	=	variation of electron kinetic energy through the sheath
$E_{i,sheath}$	=	variation of ion kinetic energy through the sheath
$E_{i,ionization}$	=	the first ionization energy of xenon
E_{wall}	=	electric field at the emitter surface
I_D	=	discharge current
J	=	emitted current density
k	=	Boltzmann constant
m_e	=	electron mass
m_i	=	ion mass
$\dot{m}$	=	mass flow rate
n_e	=	electron density
n_i	=	ion density

[1] Ph.D student, Beihang university school of astronautics, caoshuai@buaa.edu.cn.
[2] Associate professor, Beihang university school of astronautics, rjx_buaa@163.com.
[3] Professor, Beihang university school of astronautics, thb@buaa.edu.cn.

n_n	=	background gas density
N_e^-	=	number of electrons absorbed by emitter surface
N_{XE}^+	=	number of ions impacting emitter surface
$N_{emission}$	=	number of emitted electrons
P_{total}	=	background total pressure
$\dot{q}_e$	=	electron energy flux deposited on emitter surface
$\dot{q}_i$	=	ion energy flux deposited on emitter surface
$\dot{q}_{emission}$	=	emitted electron energy flux
T	=	emitter temperature
T_e	=	electron temperature
T_i	=	ion temperature
T_n	=	background gas temperature
v_e	=	velocity of electron
v_i	=	velocity of ion
V_p	=	plasma potential
α, β	=	empirical constant
ε_0	=	permittivity of vacuum
Δt	=	time step
φ_{SH}	=	Schottky potential
φ_{sheath}	=	sheath potential
φ_{wf}	=	emitter work function

I. Introduction

Hall thruster and Ion thruster have been widely used along with the development of related technologies[1,2]. As a significant component of these two kinds of thrusters mentioned above, hollow cathode can directly affect the whole propulsion system's function of a spacecraft. Furthermore, the emitter (or insert) region of hollow cathode is the main internal area where electrons and ions are generated. Consequently it's important to study the interior physical mechanism and the optimization design of hollow cathode.

The hollow cathode has advantages of enhanced current density and high ionization efficiency because of its closed structure[3]. Hollow cathode can be used in plasma contactor, Ion or Hall thrusters as a discharge or neutralizer cathode[4,5,6]. At the same time, however, it's difficult to measure the plasma parameters in the insert region, which suggests that numerical simulation can be very useful to study the inner physical characteristics and working mechanism.

In previous studies, most of simulation work focused mainly on the fluid model. Ira Katz et al[2] came up with an one-dimensional hollow cathode model. Mikellides et al[7] presented a two-dimensional axisymmetric theoretical model of the multispecies fluid inside a 1.2-cm-diam hollow cathode insert region. The complex theoretical model and experiment efforts predicted the heavy species temperatures as high as 2034K and the potential drop near the emitting surface less than 8V while extended governing equations were taken into account. Numerical simulations results showed that approximately 13.4A electron current, and 4.39A ion current transferred to the emitter surface with the hollow cathode operating at a mass flow rate of 5.0sccm and discharge current of 25.0A. The highest insert temperature reached 1450K with the 37.6A emitted electron current[4,5]. They had also investigated the anomalous heating of the plasma near the orifice by comparisons with the measurements. Meanwhile, JPL developed a 2D-axisymmetric and time-dependent computer code (OrCa2D and IROrCa2D) to compute the plasma parameters of hollow cathode, which neglected the time-dependent terms in the plasma conservation equations and the neutral gas dynamics on the assumption that the electron density was equal to the ion density[4,5,6]. Based on the results calculated by the fluid model of the plasma inside the insert region, Ira Katz et al then created a thermal model to study the heating mechanisms and the distribution of temperature in emitter region[8,15]. According to this thermal mode, ions and electrons could effectively heat the emitter to maintain thermionic electron emission by impacting the walls. As the orifice size increased from type A to type C, the plasma density, emitter temperature, plasma heating fluxes towards the emitter, plate and orifice wall had noticeable changes[15]. And some previously published simulation models and experiments also supported the aforementioned work, which indicated that the insert temperature may be used to predict the emitter life before practical application.

Levko et al[9,10] used a self-consistent two-dimensional particle-in-cell (PIC) simulations with Monte-Carlo collision to study an orificed hollow cathode operating in a planar diode geometry. Although the xenon background gas density was artificial, the ions and electrons were treated as particles. Different collision processes, electron emission with Schottky enhanced effect, and secondary electron emission from cathode walls caused by ion bombardment were all taken into consideration[9]. They employed the PIC codes to discuss the cathode plasma parameters including the distributions of velocity, potential, plasma density, and energy flux towards the walls at different operating points of orifice size, discharge voltage, and gas pressure. The results showed that the gas discharge or ionization firstly happened outside the insert region. Then the generated ions propagated upstream and penetrated inside the orifice and insert regions. As a consequence, a positive bias potential relative to the emitter and plate which exceeded the Xe first ionization energy occurred inside the insert region. It indicated that then the bulk plasma could also be generated inside the insert region. The PIC-MCC simulation showed that the energy distribution of electrons deviated from Maxwellian distribution function inside the insert region. And the energy of ions could reach tens of eV by the sheath acceleration which may result in the sputtering erosion of the emitter. Then they used their PIC-MCC simulation model to study the influences of $Xe2^{+}$ ions and excited Xe^{*} atoms on the micro-hollow cathode discharge[10]. Simulation results of the plasma and sheath parameters were discussed detailedly.

Sary et al[11,12] from university of Toulouse developed a two-dimensional axisymmetric quasi-neutral fluid model of a hollow cathode with the neutrals, ions and electrons all taken into consideration. They applied a thermal model accounting for the self-heated regime of the cathode into the gas discharge process, and presented an enhanced model of electron transport in the plume to explain the streaming or ion acoustic instabilities[11,12]. The simulated plasma density agreed well with experimental data in the insert region while the plasma potential had a qualitative agreement. Some boundary conditions chosen in this paper like the inlet were different from JPL fluid model[4,5] for the particle movement. The electron–ion coulomb collision, CEX collision and ionization collision were all coupled into the gas discharge model to give a detailed description of HC discharge. Besides, they proposed a new emissive sheath model[11] including the space charge limitation effect, which could inhibit the thermionic electron emission and largely influence the transports of electrons and ions from bulk plasma to the emitter. Combined with the Schottky effect and porous emitter surface, the emissive sheath could give a comprehensive understanding of the thermionic emission process. Parameter studies including gas pressure, plasma potential oscillations, current balance, and emitter temperature were also conducted to investigate the influences of different operating points[12].

The studies presented above give an integrated explanation about hollow cathode insert region, including experiments, theories, and numerical simulations using fluid or PIC method. Researchers attempted to understand the complicated physical process, heating mechanism, thermal model, and some other significant problems referring to HC discharge. However, specialized research on particle behaviors corresponding to different orifice sizes was not deeply introduced. So few works used particle simulation to give a detailed analysis of particle behaviors and emitter energy deposition associated with different orifice sizes. Further studies established on PIC numerical simulation method are needed to acquire more information about the micro-processes of particles in insert region. In order to study the plasma characteristics of hollow cathode insert region, in this paper some critical parameters are investigated by using a 2D axisymmetric particle-in-cell (PIC) model combined with Monte-Carlo collisions. PIC-MCC method allows us to track the particle's motion and store the information of all computed particles. The physical features captured by the PIC-MCC model including the distribution of plasma potential, density and heating flux towards the emitter, were calculated with different orifice sizes. The HC operated at the same point of 13.0A discharge current and 3.7sccm gas flow when the orifice size changed. An increased permittivity as well as an artificial mass ratio was used in the PIC-MCC code to lower the computational cost and expedite the convergence process.

II. Physical model

The simulation geometry used in our PIC-MCC model is illustrated in Fig 1. For the purpose of validating the PIC-MCC simulation used in this paper by making a comparison with fluid model, the hollow cathode insert region enclosed by the walls was simplified referring to the computational domain of NSTAR HC fluid model[5]. The 2D PIC-MCC simulation was carried out for a hollow cathode insert region with an inner diameter of 4 mm, emitter length of 10 mm, and orifice size or diameter of 2~3.5 mm. The electrons and ions were treated as particles while the neutrals had a background density distribution and uniform temperature.

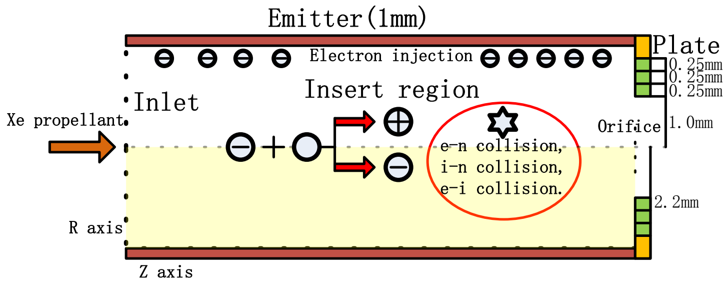

Figure 1. Schematic picture of the computational region.

A. Theoretical model of the emitter

The thermionic electron emission can be described by Richardson-Dushman law[13]

$$\mathrm{J} = \mathrm{D}T^2 \exp\left(-\frac{e\varphi_{wf}}{kT}\right) \exp\left(\frac{e\varphi_{SH}}{kT}\right) \tag{1}$$

$$\varphi_{SH} = \sqrt{\frac{eE_{wall}}{4\pi\varepsilon_0}} \tag{2}$$

$$\varphi_{wf} = 1.41 + 5 \times 10^{-4} T \tag{3}$$

E_{wall} accounting for the Schottky field-enhanced emission effect[7,9] is the electric field at the emitter surface. According to Eq. (1), the emitted electron current density J depends on the emitter temperature and work function. The distribution of the insert temperature T (in Kelvin) used in this model, which refers to the experimental data[5,14], is non-uniform. And the work function is only determined by emitter material for a certain temperature[7], as indicated in Eq. (3).

In the fluid model, assuming that electrons leaving the bulk plasma follow a Maxwellian distribution, then the average energy loss of electron from bulk plasma to the emitter surface can be described by

$$E_{e,kinetic} = \frac{2kT_e}{e} + \varphi_{sheath} \tag{4}$$

The ions are accelerated from bulk plasma to the sheath boundary by pre-sheath with Bohm velocity ($\frac{T_{eV}}{2}$). So the plasma potential could be approximated as

$$V_p \approx \frac{kT_e}{2e} + \varphi_{sheath} \tag{5}$$

And the kinetic energy deposited on the emitter by each ion is equal to

$$E_{i,kinetic} = \frac{kT_e}{2e} + \varphi_{sheath} \tag{6}$$

Combined with the practical collision processes occurring between charged particles and the walls, the energy flux exchanges are given by

$$\dot{q}_{i,n} = (E_{i,sheath} + \frac{kT_{e,n}}{2} + E_{i,ionization} - e\varphi_{wf})(\frac{N_{Xe^+,n}}{A\Delta t}) \tag{7}$$

$$\dot{q}_{e,n} = (-E_{e,sheath} + e\varphi_{sheath} + 2kT_{e,n} + e\varphi_{wf})(\frac{N_{e^-,n}}{A\Delta t}) \tag{8}$$

$$\dot{q}_{emission,n} = -(e\varphi_{wf})(\frac{N_{emission,n}}{A\Delta t}) \tag{9}$$

$$E_{i,sheath} = E_{e,sheath} = e\varphi_{sheath} \tag{10}$$

$$E_{i,ionization} = 12.1eV, \varphi_{wf} = 2.16V \tag{11}$$

Ions from bulk plasma are accelerated by the potential drop φ_{sheath} in the sheath and then release their kinetic energy ($\frac{kT_{e,n}}{2e}$) to the insert surface. At the same time, partial energetic electrons can overcome the sheath barrier and be absorbed by the emitter. Therefore, both plasma electrons and ions can serve as heat sources for the emitter.

In this paper, the energy fluxes deposited on the emitter surface are computed using the following equations

$$\dot{q}_{i,n} = (E_{i,kinetic} + E_{i,ionization} - e\varphi_{wf})(\frac{N_{Xe^+,n}}{A\Delta t}) \tag{12}$$

$$\dot{q}_{e,n} = (E_{e,kinetic} + e\varphi_{wf})(\frac{N_{e^-,n}}{A\Delta t}) \tag{13}$$

$$E_{i,kinetic} = \frac{1}{2} m_i v_{i,n}^2, E_{e,kinetic} = \frac{1}{2} m_e v_{e,n}^2 \tag{14}$$

Assuming that electrons and ions are entirely absorbed when they impact the emitter surface, the wall is able to receive all the kinetic energy of each impacting ion or electron. The neutrals do not contribute considerable energy to the walls, because the background gas temperature is not much higher than the emitter temperature. Then we can directly obtain the heating flux of electrons and ions as Eq. (12) and Eq. (13) respectively in our PIC-MCC model by means of recording the number flux and total kinetic energy delivered to the wall from each particle.

B. Boundary conditions

The boundary conditions used in our PIC-MCC model are shown in Fig 2. The cathode was grounded to have a 0V reference potential. The potential at the orifice entrance was set to a constant value of 15V. As a consequence, the emitted electrons were attracted by a positively biased orifice downstream of the computational region. Meanwhile, the emitted electrons could get sufficient energy exceeding 12.1eV to ionize the xenon gas propellant. Besides, the cathode operated at a gas flow of 3.7sccm and discharge current of 13.0A to have a quantitative contrast with literatures[15].

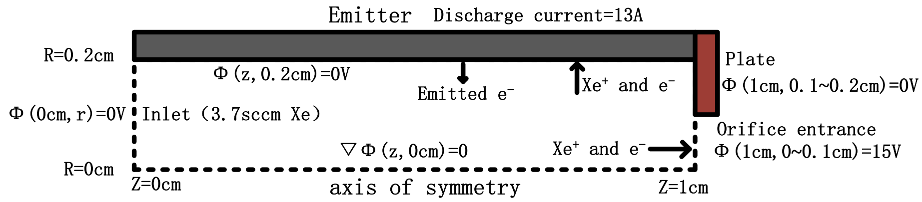

Figure 2. Operating and boundary conditions used in the model.

To estimate the background pressure distribution, an empirical formula of gas pressure for a mercury Hollow cathode[16] was adopted as Eq. (15) when we neglected orifice plate thickness effect.

$$P_{total} = (\frac{\dot{m}}{d_0^2})(\beta + \alpha I_D) \times 10^{-3} Torr \tag{15}$$

$$n_{n,n} = \frac{P_{total} - (n_{e,n} k T_{e,n} + n_{i,n} k T_{i,n})}{k T_n} \tag{16}$$

Where propellant mass flow rate $\dot{m}$ is in mA equivalent and orifice diameter d_0 is in mm. Although Eq. (15) is served for mercury propellant, we can qualitatively see that gas pressure P is proportional to $\dot{m}/d_0^2$ and linearly increases with discharge current I_D, which could help to calculate the background pressure with different operating points and design choices for a Xe hollow cathode. Once the operating point including mass flow rate and discharge current is confirmed in the PIC-MCC model, the background pressure can be easily solved with different orifice sizes. In the PIC code, the background total pressure was determined according to the reference[17]. Taking into consideration the partial pressure from charged particles which can be easily calculated in the PIC code and assuming that the neutral gas obeys the ideal-gas law, one can obtain the neutral particle density as Eq. (16). In our PIC-MCC model, we assumed that the neutral gas had uniform temperature (approximately 1500K) which was set to equal to the wall temperature. The emitter had a non-uniform temperature distribution which was set to an experimentally measured profile[5,14]. When the orifice size increased, in the PIC-MCC code the background gas temperature and the emitter temperature were thought to change linearly by using constant coefficients until the HC operated at the same discharge current.

It's worth pointing out that unlike the 2D-fluid computational domain with zero-thickness sheath boundary condition[4,7], the grounded wall boundaries used in our PIC-MCC model had the uniform potential of 0V. Both the emitter and plate were considered to be an idealized charge collector, which indicated that the electrons would be deposited at the wall surface while the ions would recombine the electrons at the wall boundaries and then turn back to the computational region as neutral particles.

C. Collisions

The dominant mechanisms which determine the transport of particles (electrons and ions) are related to different types of collisions. The collisions modeled in this effort occurred between electrons and neutrals (e-n), ions and neutrals (i-n), electrons and ions (e-i). The selection of collisions was based on the analysis of mean free path[18]. MCC methodology was used in the PIC code to handle the collision process. The primary collisions simulated in this paper include

Ionization reactions: $\mathrm{e} + \mathrm{Xe} \rightarrow \mathrm{e} + \mathrm{X}e^{+} + e$

Neutral excitation collision: $\mathrm{e} + \mathrm{Xe} \rightarrow \mathrm{e} + \mathrm{X}e^{*}$

Charge exchange collision: $\mathrm{X}e^{+} + \mathrm{Xe} \rightarrow \mathrm{Xe} + \mathrm{X}e^{+}$

Three-body recombination collision: $\mathrm{e} + \mathrm{X}e^{+} + e \rightarrow \mathrm{e} + \mathrm{Xe}$

The currently adopted electron-neutral collision cross sections against a Maxwellian electron energy distribution, combined with the electron-ion and ion-neutral collision cross sections were consulted from the literatures[19,20,21]. It is important to note that the charge exchange collision could deeply influence the kinetic energy and number of ions deposited on the emitter surface.

III. Numerical method

The motions of electrons and ions follow Newton's second law.

$$m_i \frac{d\vec{v_i}}{dt} = q_i(\vec{E} + \vec{v_i} \times \vec{B}) \tag{17}$$

$$\frac{d\vec{x_i}}{dt} = \vec{v_i} \tag{18}$$

Where vector $\vec{x_i}$ represents displacement. Subscript i means the charged particle species (e^- or Xe^+). Poisson equation was used in the PIC code to solve for the distributions of potential and electric field.

$$\nabla^2\varphi = -\frac{e(n_i - n_e)}{\varepsilon_0} \tag{19}$$

$$\frac{\partial^2\varphi}{\partial r^2} + \frac{1}{r}\frac{\partial\varphi}{\partial r} + \frac{\partial^2\varphi}{\partial z^2} = -\frac{e(n_i - n_e)}{\varepsilon_0} \tag{20}$$

$$\mathrm{E} = -\nabla\,\varphi \tag{21}$$

When used in the two-dimensional axisymmetric model, the Poisson equation can be written as Eq. (20).

Both increasing permittivity ($25 \times 25\varepsilon_0$) and an artificial mass ratio ($0.01m_i$) which have been proven to be very effective[18,22,23] were used to reduce computation cost and accelerate the convergence process in the PIC code. In this case, necessary corrections needed to be conducted to obtain the reasonable results. The electric field E_{wall} at the emitter surface used in Eq. (2) could be directly computed in the PIC code. Because the increased permittivity (25×25 times) not only enlarged the Debye length and sheath thickness but also weaken the electric field at the emitter surface, E_{wall} needed to be increased by 25 times in the PIC code so as to figure out the true Schottky effect and emitted current density.

The null collision handling method was used for the procedure of Monte-Carlo collision[24]. The program flowchart for the solution of PIC-MCC model is described in Fig 3. And the procedure was carried out repeatedly until the simulation results of all plasma parameters and operating quantities reached the steady state.

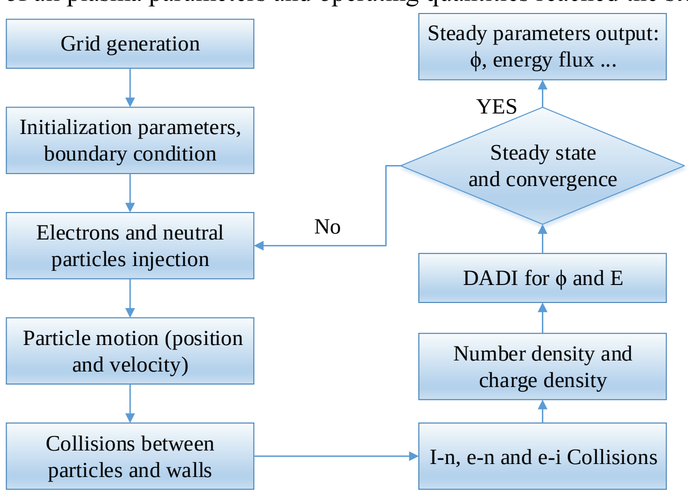

Figure 3. Schematic of PIC-MCC numerical approach.

IV. Results

A. Discharge characteristics

This section shows the HC discharge parameters simulated by the 2D PIC-MCC model at a gas flow rate of 3.7sccm and discharge current of 13.0A, which are compared with the results obtained by the fluid model and experimental data. In the model, the neutrals are considered as a background rather than simulated particles. The neutral gas pressure and density are determined according to ideal gas law. And the temperature of the neutral gas is assumed to be equal to the average wall temperature of 1500 K.

As can be seen in Fig 4, the simulation results have converged after 400,000 calculation steps (about 2μs) when the number of charged particles (1.3×10^{12} e^- and 1.65×10^{12} Xe^+) and discharge current (~13A) reach the steady state. The number of ions is slightly larger than the number of electrons because electrons have a greater mobility rate.

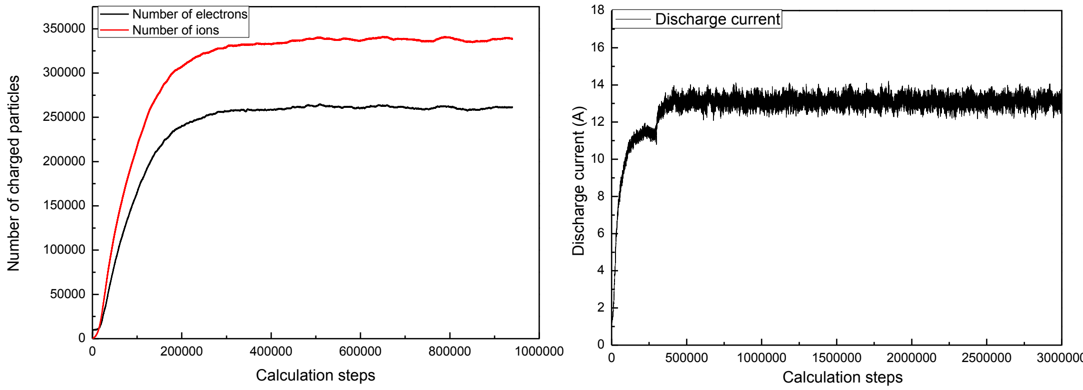

Figure 4. Statistics on computed macro-particle quantities (a, left side), and discharge current (b, right side) variation with respect to calculation steps.

Fig 5 shows the electron and ion current from plasma zone to the emitter at the operating point of 3.7sccm mass flow rate and 13.0A discharge current. The average electron current and ion current imparted to the emitter and plate wall are 14.3A, 1.05A and 1.2A, 0.27A respectively. We can easily see that the majority of the emission current returns to the wall while partial ions generated from gas ionization are accelerated from bulk plasma to the emitter surface by sheath. In this process, electrons and ions would certainly release the particle kinetic energy to the emitter surface. In particular, one critical point needs to be underlined that the wall boundaries applied in this PIC-MCC model were grounded with a constant potential rather than the zero-thickness sheath boundary used in the fluid model[4,7]. It suggests that an emissive sheath[11] associated with a potential barrier between bulk plasma and the emitter surface could not only attract more ions from ionization region to the wall but also prevent some emitted electrons drifting to the bulk plasma, because of the thermionic emission limited and space charge saturated regimes[11]. As a result, the electron and ion backflows are probably lager than the results derived from the fluid model.

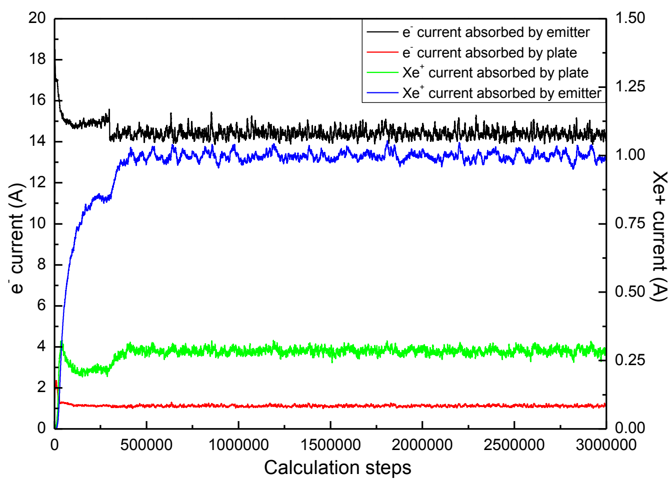

Figure 5. Electron current and ion current absorbed by emitter and plate with respect to calculation steps.

The potential distribution overlaid by gradient lines starting from the orifice entrance and ending at other boundaries is depicted by the contour in Fig 6. The gradient lines are used to represent the direction of the electric field and account for the movement of charged particles. The ionization region close to the axis of symmetry and orifice entrance locates at the area where the electric potential is relatively high. So ions would be accelerated to hit the emitter, which means the potential energy obtained in the electric field would be deposited on the insert surface. At the same time, abundant electrons would flow out of the insert region from the orifice entrance and then enter the plume region so as to provide an electron current source for the thruster.

The potential distribution of the insert region is crucial for understanding how charged particles are produced and then move out of the computational domain in a PIC-MCC model. The particle-in-cell code may be validated by a comparison between the potential computed by the 2D PIC-MCC model and the experiment data. As can be seen in Fig 6, the simulated potential trend by particle model could qualitatively agree with the experimental result[5] within 10mm from the orifice entrance. We want to emphasize that the energy of the emitted or bulk plasma electrons is not sufficient enough to overcome the first ionization potential barrier (about 12.1eV), though only a small portion of electrons may have higher energy derived from Maxwellian high-energy tail. According to the literature[9], at the beginning the thermionic emission electrons could not ionize the gas inside the HC, which indicated that the gas discharge firstly happened outside the insert region because of the high potential from the keeper or anode. Then the generated plasma propagated upstream inside the insert region accompanied with a positive bias potential which exceeded the gas ionization energy. At last, the bulk plasma could also be generated inside the insert region. In order to have a dense plasma in the hollow cathode insert region, a relatively higher artificial voltage (15V in this paper) needed to exist at the orifice entrance in our PIC-MCC model.

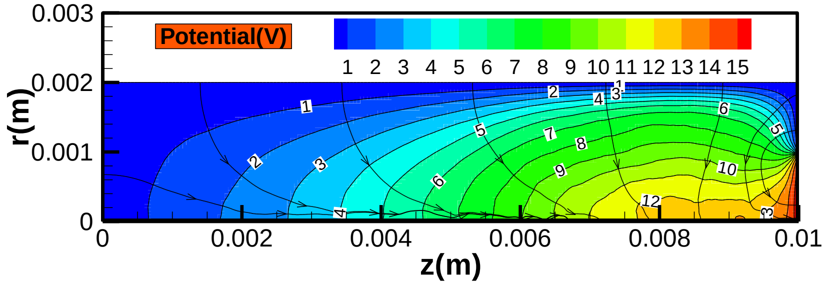

Figure 6. Potential distribution and gradient lines.

Fig 7 shows the plasma density distribution. The highest plasma density could reach the magnitude of 8e19m^{-3} at the operating point of 13.0A discharge current and 3.7sccm gas flow rate when the orifice diameter is 2mm. The ionization region appearing with the highest plasma density is located nearby the orifice entrance, because in this area the emitted electrons have been fully accelerated by the electric field and the kinetic energy of the single electron is relatively higher so as to exceed the first ionization energy of Xe propellant. As a matter of fact, the number density of electrons almost equals to that of ions ($n_i \approx n_e$) due to Debye shielding effect especially in the ionization or bulk plasma region, which means the majority of plasma in the insert region could be seen as a quasi-neutral flow. However, the density difference of electrons and ions nearby the emitter surface becomes larger, which can be explained by the fact that the emissive sheath connecting the emitter surface and the bulk plasma may deeply influence the transport and diffusion of charged particles. Besides, in the sheath the electrons come from both the ionization region and the thermionic emission surface while the ions are mainly motivated from the bulk plasma.

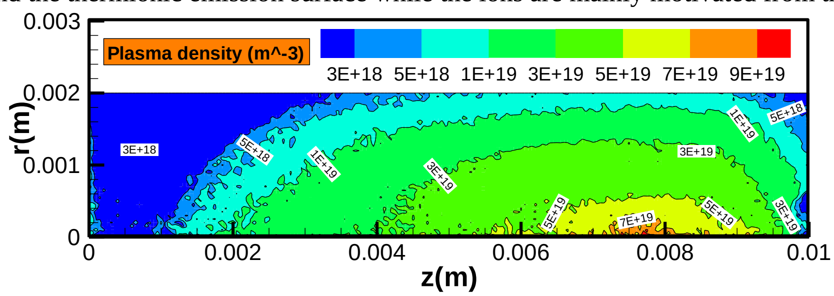

Figure 7. Plasma density distribution.

The emitter temperature profile set in the PIC-MCC simulation model referred to the experimental curve[5,14] which indicated that the temperature distribution along the emitter surface was non-uniform. As revealed by Fig 8, The Schottky effect combined with porous emitter surface[5,11] could significantly enhance the practical emitted current density. The net enhanced emitted current density described as the blue curve in Fig 8 is the difference between the Richardson-Dushman law with and without Schottky and porous surface effect. The tendency of these curves tells us that the highest emitted current density occurs nearby the cathode plate. Actually, according to the literatures[5,14] the highest emitter temperature is located at the downstream boundary of the computational domain which is closest to the orifice plate. Meanwhile, the simulated electric field of radial direction along the emitter surface gradually increases as a function of the axial coordinate Z(m) until the location of the ionization region, where the potential drops dramatically from bulk plasma to the emitter surface as shown in Fig 6. These factors mentioned above may help to account for the variation tendencies of the curves in Fig 8.

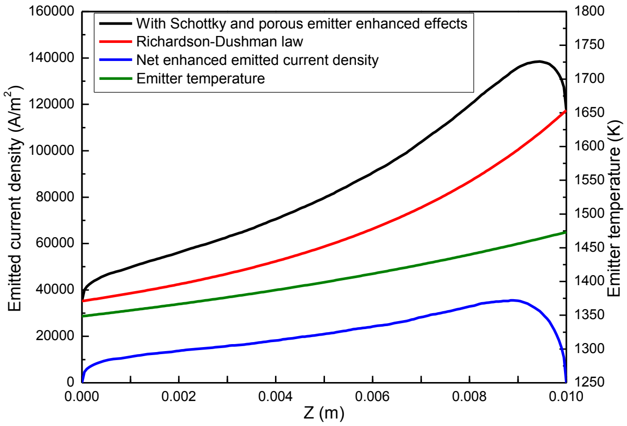

Figure 8. Emission current density and temperature along the emitter surface with a 2mm orifice size.

B. Plasma parameters with different orifice sizes

As described in Fig 9, the plasma region is located near the orifice entrance because of the higher potential. As the orifice size increases, we can clearly see that the plasma particle position would propagate upstream in the insert region. Ions move from the ionization region to the emitter, cathode tube and orifice plate while the electrons are mainly transported to the emitter and orifice entrance. These particle motions involved in the self-sustained equilibrium process of HC may help to heat the emitter directly or through thermal conduction from the tube and plate. Fig 10 shows the radial velocity of all computed ions and electrons with respect to particle location. We can easily see that the ions from ionization region are accelerated to impact the emitter with the highest radial velocity of 4500m/s, which is certainly beneficial for depositing more energy on the emitter surface. For the case of 2mm orifice size, the axial position of the largest Xe^+ radial velocity is close to the orifice entrance and plate, while the magnitude and direction of e^- radial velocity (within ±3e6m/s) have a relatively uniform distribution in the whole area.

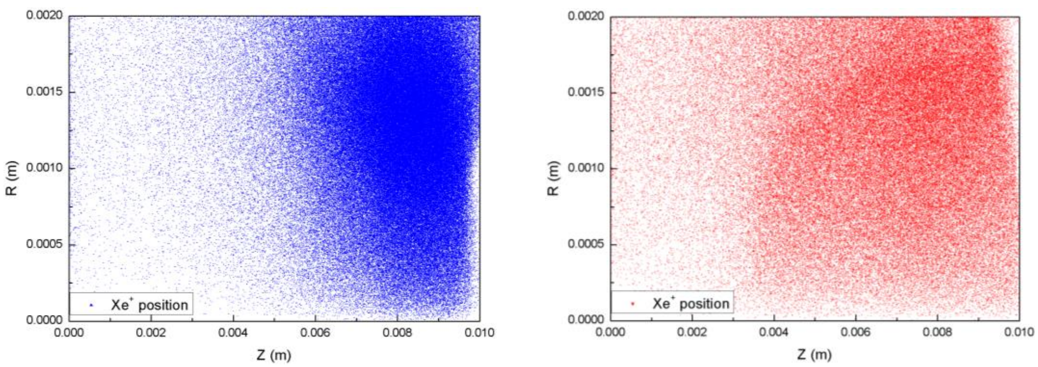

Figure 9. Plasma position distribution for different orifice sizes of 2mm (a, left side) and 3.5mm (b, right side).

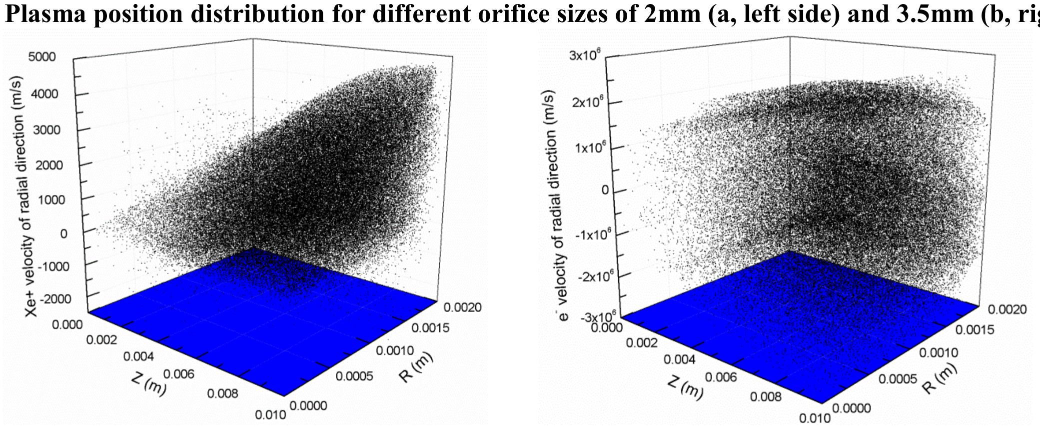

Figure 10. Statistics on the radial velocity of all calculated ions (a, left side) and electrons (b, right side) with respect to particle location.

Fig 11 shows the plasma potential variations along the symmetry axis and R direction at the same operating point. As the orifice diameter increases from 2.0mm to 3.5mm, the high plasma potential region moves upstream in the insert region at the axial direction while the radial potential variation from the symmetry axis to the emitter surface becomes faster and larger. This phenomenon could be explained by the fact that the ionization region expands upstream in the computational domain as noted in Fig 9 when the orifice size increases. As shown in Fig 11(a), the sheath potential or the potential barrier between the bulk plasma and the emitter surface has an apparent increase as the reference[13]. Consequently, the quasi-neutral bulk plasma area associated with the relatively high potential begins to enlarge from the orifice entrance to the emitter, plate and left boundary with the increase of the orifice size. In this paper the inlet boundary was set to a constant reference value of 0V, which may result in the differences of potential and density distribution with the references[4,5] in the left side of the insert region.

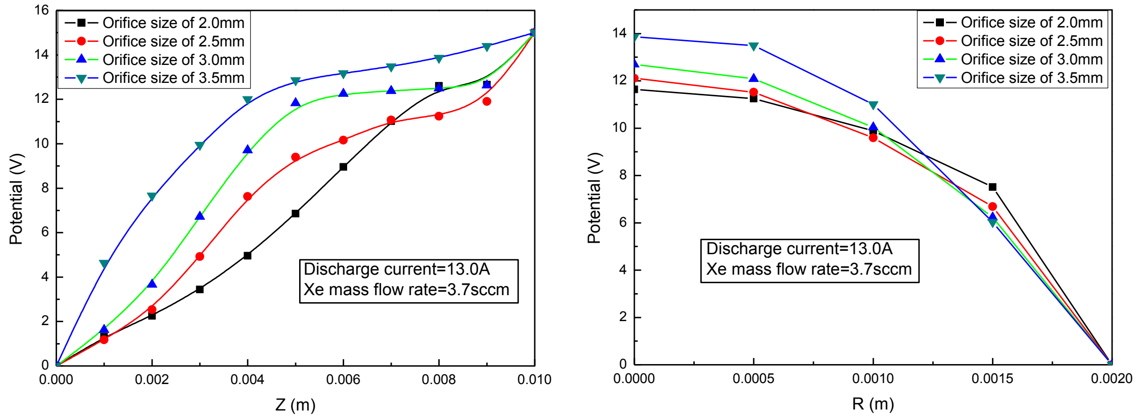

Figure 11. Potential variations versus different orifice sizes along Z axis (a, left side) and R axis (b, right side).

A non-monotonic tendency is exhibited by the Xe^+ density along the hollow cathode central axis, which is in accordance with the fluid model and previous experimental data[4,7], as shown in Fig 12. As the orifice diameter increases at a given gas flow rate and discharge current, the axial location of the gradually decreasing peak ion density moves upstream in the insert region. And in the left side of the computational domain, the plasma density has a rising tendency. It's easy to draw our attention that the similar varying patterns could also be found in (b) of Fig 12 revealing the ion density variation along the emitter. As it has been proved, the ionization region or bulk plasma would move upstream when orifice size increases, which is in accordance with the variations in Fig 12. The ion density variation versus different orifice sizes along R axis (Z=0.008m) is shown as (b) of Fig13. We can easily see that there is a strictly decreasing trend of ion density with the increase of radial coordinate R(m) because the bulk plasma area is located at the center of the gas channel. When the orifice size increases, the ionization region associated with the highest plasma density moves upstream and keeps away from orifice entrance. In addition, the ion density radial variation is captured at the axial position of 0.008m which is very close to the orifice entrance. So the ion density at the same axial position has a consistently decreasing tendency as the orifice size increases.

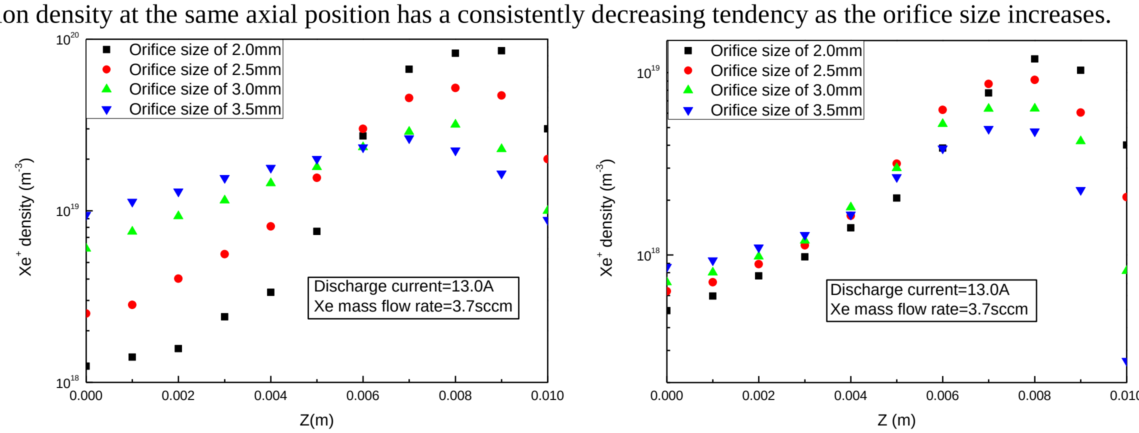

Figure 12. Ion density variation versus different orifice sizes along symmetry axis (a, left side) and emitter surface (b, right side).

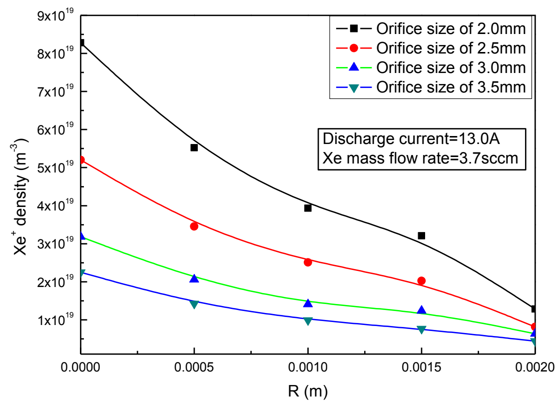

Figure 13. Ion density variation versus different orifice sizes along R axis.

The emitter is directly heated by the fluxes of ions and electrons accompanied by the process of energy deposition from bulk plasma to the emitter surface. In order to assess the effect of the surrounding plasma environment on the emitter energy equilibrium, the particle and heating fluxes delivered to the emitter surface need to be determined quantitatively. Fig 14 shows the heat fluxes by electrons and ions versus different orifice sizes along Z axis at the same operating point. As the orifice diameter increases, the peak heat flux derived from electrons reduces sharply, while the heat flux caused by ion bombardment along the whole emitter surface including the peak value increases significantly. This matter may be caused by the incremental potential barrier in the emissive sheath which could attract more ions and suppress more electrons from bulk plasma to the emitter surface. A same variation tendency, however, can be easily seen that both the locations of peak heat flux from electrons and ions move upstream when the HC has a larger orifice size. It could be easily understood that this trend appears in concert with the movement of the ionization region. Besides, the simulated heating fluxes of electrons and ions are larger than the results of fluid model[15], which can be explained by the increased electron and ion backflows as noted in Fig 5.

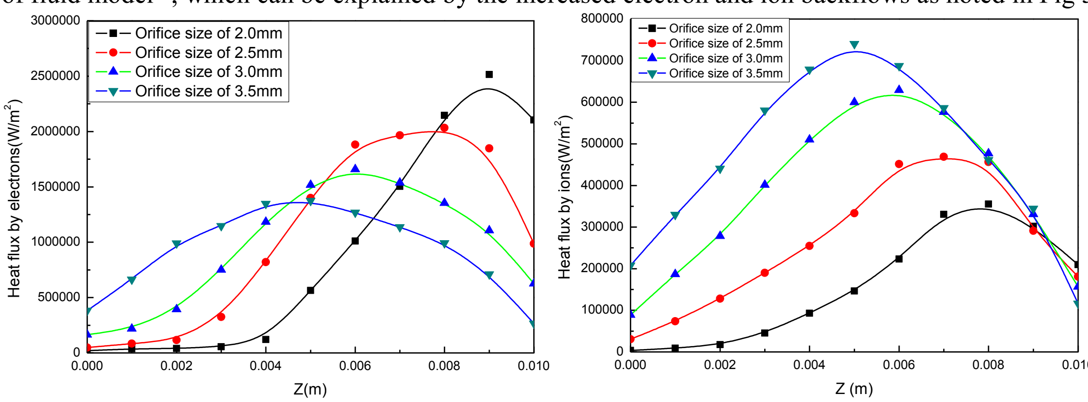

Figure 14. Energy flux deposition on emitter by electrons (a, left side) and ions (b, right side) versus different orifice sizes along Z axis.

V. Discussion

The computational domain used in our PIC-MCC model mainly concentrated on the hollow cathode insert region with different orifice diameters switching from type B to type C. The orifice sizes of type A were not taken into consideration because the considerably high gas pressure and plasma density may largely increase the number of computational grids as well as the time consumption. In the next step, we plan to employ the self-similar methodology and the hybrid-PIC model to conduct deeper researches on the orifice sizes of type A and the pint-sized hollow cathode used for the micro electric thruster.

The equations[8] with regard to energy fluxes used in fluid model were based on the assumptions that electrons leaving the plasma were characterized by a Maxwellian distribution function and the sheath enclosing the emitter surface was a collision-free path for charged particles. Under these hypotheses, the electrons and ions arriving at the emitter surface could ideally implement energy depositions as described in those equations (Eq. (4) to Eq. (8)). Taking into account a single electron's practical transport and diffusion process with complicated collisions, a 0D theoretical energy model may not be able to account for the accurate movement and actual energy state of each electron or ion. However, PIC-MCC particle simulation used in this paper can record the exact quantities of particles impacting the walls and the concrete value of energy carried by each electron or ion anywhere and anytime. Regardless of whether the bulk plasma Maxwellian distribution is satisfied or not, we are able to know the specific kinetic energy deposited on the emitter surface from every single particle impacting the emitter (as indicated in Eq. (12) and Eq. (13)). As revealed by Fig 15, the electron energy distribution function (EEDF) obtained by the PIC-MCC model deviates from the Maxwellian distribution function.

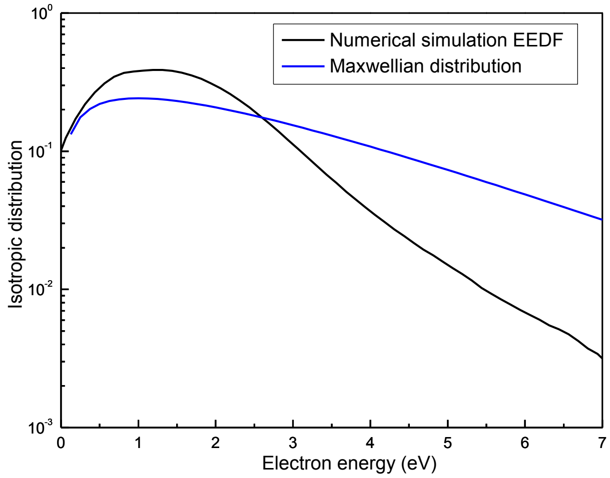

Figure 15. Electron energy distribution function with comparison to Maxwellian distribution.

When the orifice size is small, the thermionic electron emission and energy fluxes transported to the emitter surface mainly concentrate on the location near the plate, which may result in a faster dissipation rate of emitter material as well as an excessively high local temperature. Because the HC lifetime is greatly determined by the evaporation rate of the emitter material[8] which has a remarkable dependence on the emitter operating temperature, the lifetime of the HC with a small orifice size may be largely reduced. But when the HC has a larger orifice size with the same operating point, the distribution of heat fluxes carried by electrons and ions becomes considerably dispersive within the whole insert region. In this case, the emitter temperature would have a more uniform distribution while the peak insert temperature would markedly decrease. As a consequence, more emitter surface area could serve as a thermionic emission source and the HC would have a longer lifetime. As indicated in (b) of Fig 14, however, more ions coming from bulk plasma could provide largely improved heat flux for the emitter surface because of the enlarged sheath potential difference when the orifice diameter increases. Another factor needs to be highlighted that the collision frequency of charge exchange (CEX) which can significantly lower the ion kinetic energy goes down as the orifice increases, because the background density or pressure of the neutral particles drops dramatically. As a result, the HC lifetime may be shortened by the increased ion-induced sputtering erosion of the emitter. Besides, the operating points of the HC with a certain structure and the same critical sizes may deeply influence the HC discharge characteristics and the emitter lifetime, which will be further studied in our future work. So a designer needs to take all these factors into consideration in order to make a better choice about the orifice sizes and operating conditions.

VI. Conclusion

A two-dimensional axisymmetric PIC-MCC model was developed to conduct the numerical simulation of the hollow cathode discharge driven by thermionic electron emission. The HC with different values of orifice diameter operated at the point of 13.0A discharge current and 3.7sccm gas flow rate. The PIC-MCC simulation model allows one to investigate the plasma potential, density, heating flux at different locations and record the position, energy, velocity of each particle. The variation tendencies of the simulated plasma density and potential agree qualitatively with the experimental data and fluid model.

It shows that the behaviors of charged particles play an important role in the self-heating physical mechanism of the hollow cathode emitter. The energy deposition and heating flux towards the emitter surface can be derived from the bombardments of the plasma electrons and ions imparted to the insert. The Schottky enhanced effect combined with porous emitter surface could largely strengthen the thermionic electron emission while the space charge saturated regime occurring in the emissive sheath may have a contrary effect. As the orifice size increases, the distribution of emitter temperature becomes more dispersive while the peak value decreases quickly. More emitter surface area is used for electron emission, which could benefit the improvement of HC lifetime. At the same time, however, an increase in the energy of ions bombarding the emitter surface due to the enhanced potential barrier in sheath and the decline of CEX collision frequency appears with the upstream movement of the ionization region and bulk plasma. These matters could enlarge the ion induced sputtering erosion of the insert as well as the heating flux transported to the emitter surface.

Taking those factors mentioned above into consideration, one can hardly determine a reasonable orifice size of the hollow cathode. In the future, the author plans to do more researches on the HC discharge in the entire region including the orifice and plume zones with different operating points. Besides, a pint-sized HC used for the micro electric thruster in SPEPL (http://spepl.buaa.edu.cn/) would be simulated in our particle-in-cell code.

References

[1]Polk J, Dan G, Watkins R, et al, "Characterization of Hollow Cathode Performance and Thermal Behavior," 42nd AIAA/ASME/SAE/ASEE Joint Propulsion Conference & Exhibit, Sacramento, California, 2006, AIAA 2006-5150.

[2]Katz I, Anderson J R, Polk J E, et al, "One-Dimensional Hollow Cathode Model," Journal of Propulsion & Power, 2003, 19(4): 595-600.

[3]He S., Jing H., Liu S., et al, "Influence of metastable atoms in the simulation of hollow cathode discharge," Physics of Plasmas, 2013, 20(12): 1263-1270.

[4]Mikellides I., Katz I., Dan G., et al, "Theoretical Model of a Hollow Cathode Insert Plasma," American Institute of Aeronautics and Astronautics, 2004, AIAA 2004-3817.

[5]Mikellides I., Katz I., Dan G., et al, "Theoretical Model of a Hollow Cathode Plasma for the Assessment of Insert and Keeper Lifetimes," American Institute of Aeronautics and Astronautics, 2005, AIAA 2005-4234.

[6]Mikellades I., Katz I., Dan G., et al, "Hollow Cathode Theory and Model: II. A Two-Dimensional Model of the Emitter Region," Journal of Applied Physics, 2005, vol. 98, no. 10, 113303.

[7]Mikellides I G, Katz I, Dan M G, et al. "Hollow cathode theory and experiment. II. A two-dimensional theoretical model of the emitter region". Journal of Applied Physics, 2005, 98(11):2894.

[8]Katz I, Mikellides I G, Polk J E, et al. "Thermal Model of the Hollow Cathode Using Numerically Simulated Plasma Fluxes". Journal of Propulsion & Power, 2007, 23(3): 522-527.

[9]Levko D, Krasik Y E, Vekselman V, et al. "Two-dimensional model of orificed micro-hollow cathode discharge for space application," Physics of Plasmas, 2013, 20(8): 721.

[10]Levko D, Bliokh Y P, Krasik Y E, "Influence of $Xe2^{+}$ ions on the micro-hollow cathode discharge driven by thermionic emission," Physics of Plasmas, 2014, 21(4):721.

[11]Sary G, Garrigues L, Boeuf J P, "Hollow cathode modelling: I. A coupled plasma thermal two-dimensional model," Plasma Sources Science & Technology, 2017, 26 (055007).

[12]Sary G, Garrigues L, Boeuf J P, "Hollow cathode modeling: II. Physical analysis and parametric study," Plasma Sources Science & Technology, 2017, 26(055008).

[13]D. Goebel and I. Katz, "Fundamentals of Electric Propulsion: ion and Hall thrusters," John Wiley & Sons, 2008.

[14]Polk J, Marrese C, et al, "Temperature Distributions in Hollow Cathode Emitters," AIAA Joint Propulsion Conference and Exhibit, 2004-4116.

[15]Katz I, Mikellides I G, Dan M G, et al, "Insert Heating and Ignition in Inert-Gas Hollow Cathodes," IEEE Transactions on Plasma Science, 2008, 36(5):2199-2206.

[16]Siegfried D E, Wilbur P J, "A model for mercury orificed hollow cathodes: Theory and experiment," 1984, 22(10):1405-1412.

[17]D. Goebel, K. Jameson, et al, "Hollow Cathode and Keeper-Region Plasma Measurements Using Ultra-Fast Miniature Scanning Probes," 40th AIAA/ASME/SAE/ASEE Joint Propulsion Conference and Exhibit, 2004-3430.

[18]Szabo J, Warner N, Martinez-Sanchez M, et al, "Full Particle-In-Cell Simulation Methodology for Axisymmetric Hall Effect Thrusters," Journal of Propulsion & Power, 2015, 30(1): 197-208.

[19]Hayashi M, "Determination of electron-xenon total excitation cross-sections, from threshold to 100 eV, from experimental values of Townsend's," Journal of Physics D: Applied Physics, 1983, 16(4): 581-589.

[20]Rejoub R, Lindsay B G, Stebbings R F, "Determination of the absolute partial and total cross sections for electron-impact ionization of the rare gases," Physical Review A, 2002, (65).

[21]Miller J S, Pullins S H, Levandier D J, et al, "Xenon charge exchange cross sections for electrostatic thruster models," Journal of Applied Physics, 2002, 91(3): 984-991.

[22]Szabo J. J., "Fully Kinetic Numerical Modeling of a Plasma Thruster," Ph.D. Dissertation, Massachusetts Institute of Technology, 2001, pp. 42-49.

[23]Tang H B, Cheng J, Liu C, et al. "Study of applied magnetic field magnetoplasmadynamic thrusters with particle-in-cell code with Monte Carlo collision. I. Computation methods and physical processes". Physics of Plasmas, 2012, 19(7): 754.

[24]Birdsall C K, "Particle-in-cell charged-particle simulations, plus Monte Carlo collisions with neutral atoms, PIC-MCC," IEEE Transactions on Plasma Science, 1991, 19(2): 65-85.